Available online at www.sciencedirect.com

ScienceDirect

Advances in Space Research 69 (2022) 121–131

ADVANCES IN SPACE RESEARCH
(a COSPAR publication)

www.elsevier.com/locate/asr

Effect of total lunar eclipse of 27th July 2018 on the *D*-region ionosphere by using VLF observations

Ajeet Kumar Maurya [a,*], D.V. Phanikumar [b], Rajesh Singh [c], K. Venkatesham [d] Abhay K. Singh [e]

[a] *Department of Physics, Doon University, Dehradun, Uttarakhand, India*
[b] *Department of Science and Technology, Technology Bhawan, New Delhi, India*
[c] *KSK Geomagnetic Research Laboratory, IIG, Prayagraj (Allahabad), India*
[d] *KBCAOS, University of Allahabad, Prayagraj (Allahabad), India*
[e] *Atmospheric Physics Lab, Department of Physics, Banaras Hindu University, Varanasi, India*

Received 7 January 2021; received in revised form 14 August 2021; accepted 12 September 2021
Available online 22 September 2021

Abstract

In this report, an effort for the first time has been made to investigate the effect of the total Lunar Eclipse that occurred on 27th July 2018 (the longest lunar eclipse in the 21st century) on the D-region ionosphere. Very Low Frequency (VLF) navigational transmitter signals recorded at Prayagraj (formally Allahabad) station in India is the primary dataset used. The signals from two VLF transmitters: NWC (19.8 kHz) from Australia, and JJI (22.2 kHz) from Japan, have been utilized. When compared to unperturbed night, NWC signal amplitude showed an anomalous decrease of ~0.86 dB, while JJI amplitude showed an anomalous increase ~0.26 dB during the lunar eclipse. The Wait's lower ionospheric parameters: reflection height (H') and sharpness factor (β) are estimated by using a rather coarse method of modeling of VLF signals anomalies on eclipse day, which comes out to be $H' = 85.25$ km & $\beta = 0.689$ km^{-1} and $H' = 84.59$ km & $\beta = 0.683$ km^{-1} respectively for NWC and JJI path. Using wait parameters, the electron density (N_e) profile is estimated and this showed a decrease in N_e during eclipse time with reference to the nighttime ambient values. The N_e values for the NWC path, showed relatively higher decrease compared to the JJI path. The plausible reasons for observed N_e decrease on lunar eclipse night could be due to the reflected lunar Lyman-α and X-ray's radiation which may contribute to the nighttime ionization is blocked during the lunar eclipse, thereby decreasing the nighttime lower ionospheric N_e.

Keywords: Lunar eclipse; D-region ionosphere; VLF waves; Radio remote sensing

1. Introduction

Eclipses (both Solar and Lunar) are one of the nature's spectacular celestial events always fascinating to mankind. But Solar eclipses have received enormous response from the space and atmospheric scientist due to its direct impact on the earth's atmosphere and ionosphere during daytime and hence several research papers have been published (e.g. Anderson et al., 1972; Antonia et al., 1979; Srivastava et al., 1982; Chimonas and Hines, 1970; Chimonas 1970; Maurya et al., 2014; Phanikumar et al., 2014; Singh et al., 2011). However, the effect of Lunar Eclipse (LE) on the lower ionosphere more specifically during nighttime dynamics was not very well understood because of either lack of instruments to measure such low densities and hence very few publications on this topic. Though, the search for the Lunar effect on the Earth's

* Corresponding author.
E-mail address: ajeet.iig@gmail.com (A.K. Maurya).

https://doi.org/10.1016/j.asr.2021.09.013
0273-1177/

ionosphere was a continued effort ever since the discovery of the radio propagation (e.g., Stetson, 1931; Stetson and Johnson, 1934; Banerjee and Singh, 1936; Stetson, 1944 and reference therein).

A unique study was made using group-retardation method with wave frequency of 3.8 MHz during the lunar eclipse of 08 January 1936 depicting that there was an appreciable variation in the *F*-layer ionosphere before the eclipse and the strength of the echoes appeared to be strong. However, during the eclipse, it became very weak and then regained its original strength after the eclipse, signifying the contribution of the Moon in the nighttime ionization (Banerjee and Singh, 1936). Thus, it was shown for the first time that lunar eclipse also affects the ionization of the upper atmosphere i.e. during the eclipse the ionospheric electron density may become low (Banerjee and Singh, 1936). In another interesting work by Stetson (1944), who analyzed the field intensity of WBBM Chicago at 770 kHz frequency being recorded at MIT at Boston, for the period of 10 years during 1930–1939, suggested that change in the nighttime ionization of the E-layer (~100 km altitude) was associated with changing phases of the Moon. A hypothesis was suggested that the ionizing radiation from the Moon, mainly emission of secondary X-ray radiation and reflected ultra-violet radiation, may cause the change in field intensity during night hours corresponding to the phases of the Moon.

Another aspect of studying lunar eclipse is by observing the light reflected from the surface of the Moon, the spectral features of Earth's transmission spectrum can be obtained. By calculating the brightness ratio of light reflected by the lunar surface in umbra, penumbra, and out of the eclipse, the Earth's transmission spectra can be calculated. The path length of transmission spectra is greater than the path length of reflection spectra. Earth's transmission spectra appear red and reflection spectra appear blue (Enric et al., 2009). Another observation of lunar eclipse was made on 10 December 2011 using Subaru telescope and High Dispersion Spectrogram (HDS) (Kawauchi et al., 2018). The observations were started prior to the eclipse and terminated at the middle of the eclipse. Through this observation, authors alternately got a series of spectra of sunlight reflected by two points of the lunar surface – ocean of storms and sea of fertility.

VLF signals from navigational transmitters have given us a unique opportunity to study and understand the nighttime *D*-region electron density variations during the total lunar eclipse event. The present work is first of its kind from the low latitude region. To understand the impact of 27 July 2018 total lunar eclipse on the lower ionosphere during night time, we scrutinized VLF observations from two navigational transmitters to verify any unusual ionospheric changes during the eclipse. Though Moon does not directly affect ionization as it does not have its own light, but the reflected lunar Lyman-α and X-rays radiation from lunar exosphere may be contributing as one of the minor ionizing sources during nighttime ionosphere. During lunar eclipse, these radiations are blocked and this could decrease the ionospheric ionizing radiation below ambient level.

2. VLF data and total lunar eclipse

We have utilized the very low frequency (VLF: 3–30 kHz) data recorded at a quiet location Prayagraj (formerly Allahabad) [geog. lat. 25.41°N, long. 81.93°E; geomag. lat. 16.45°N, long. 153.70°E] India, using Stanford University developed Automatic Weather Electromagnetic System for Observation Modeling and Education (AWESOME) receiver setup (Cohen et al., 2010; Singh et al., 2010). The high resolution (50 Hz) VLF data from two navigational transmitters: NWC (19.8 kHz, geog. lat. 21.82°S; geog. long. 114.17°E) from Australia, and JJI (22.2 kHz, geog. lat. 32°N; geog. long. 130.7°E) from Japan recorded at Prayagraj (PRJ) station have been utilized. The Fig. 1 shows the location of Pryagraj station, NWC and JJI VLF transmitter along with their Transmitter Receiver Great Circle Path (TRGCPs). The TRGCP path length for the NWC-PRJ path is ~6,300 km and for the JJI-PRJ path ~4785 km. We have used 1-minute average data as the lunar eclipse is long duration event and hence does not required high resolution data.

The total lunar eclipse of 27 July 2018 occurred when Moon was at its longest distance from the Sun called apogee. Hence, this is also called as apogean full Moon. At this location, Moon takes longer time to pass through the earth's shadow, compared to the full Moon when it is closer to the Earth and moving faster in the orbit. This was the longest eclipse of the 21st century. The Moon remained at least partially in the Earth's shadow for four hours and totality duration was ~1 hr 42 min 57 sec. Here, during the eclipse, the Moon passed into the center of the Earth's shadow and thus was called central lunar eclipse which occurs rarely. This eclipse was visible from the world's eastern hemisphere covering Eastern Africa, Southern Africa, Southern Asia & Central Asia and seen rising over Southern America, Western Africa & Europe and setting over Eastern Asia & Australia. The Moon during this eclipse was called 'Blood Moon' since the Moon turns red. More details about the timing of various phases of the eclipse is presented in Table 1. The eclipse details are obtained from the NASA eclipse website (https://eclipse.gsfc.nasa.gov/LEplot/LEplot2001/LE2018Jul27T.pdf). In order to show the eclipse coverage region (partial eclipse, totality, no eclipse region etc.), we have added the eclipse coverage region shown in the above mentioned pdf document from NASA lunar eclipse website as Fig. 1 (b). Further, the comparison of eclipse coverage region from Fig. 1a and PRJ-NWC & PRJ-JJI path from Fig. 1b, show that PRJ-NWC TRGCP was approximately more than half in total eclipse, whereas PRJ-JJI TRGCPs were less than 1/3 part in the totality region.

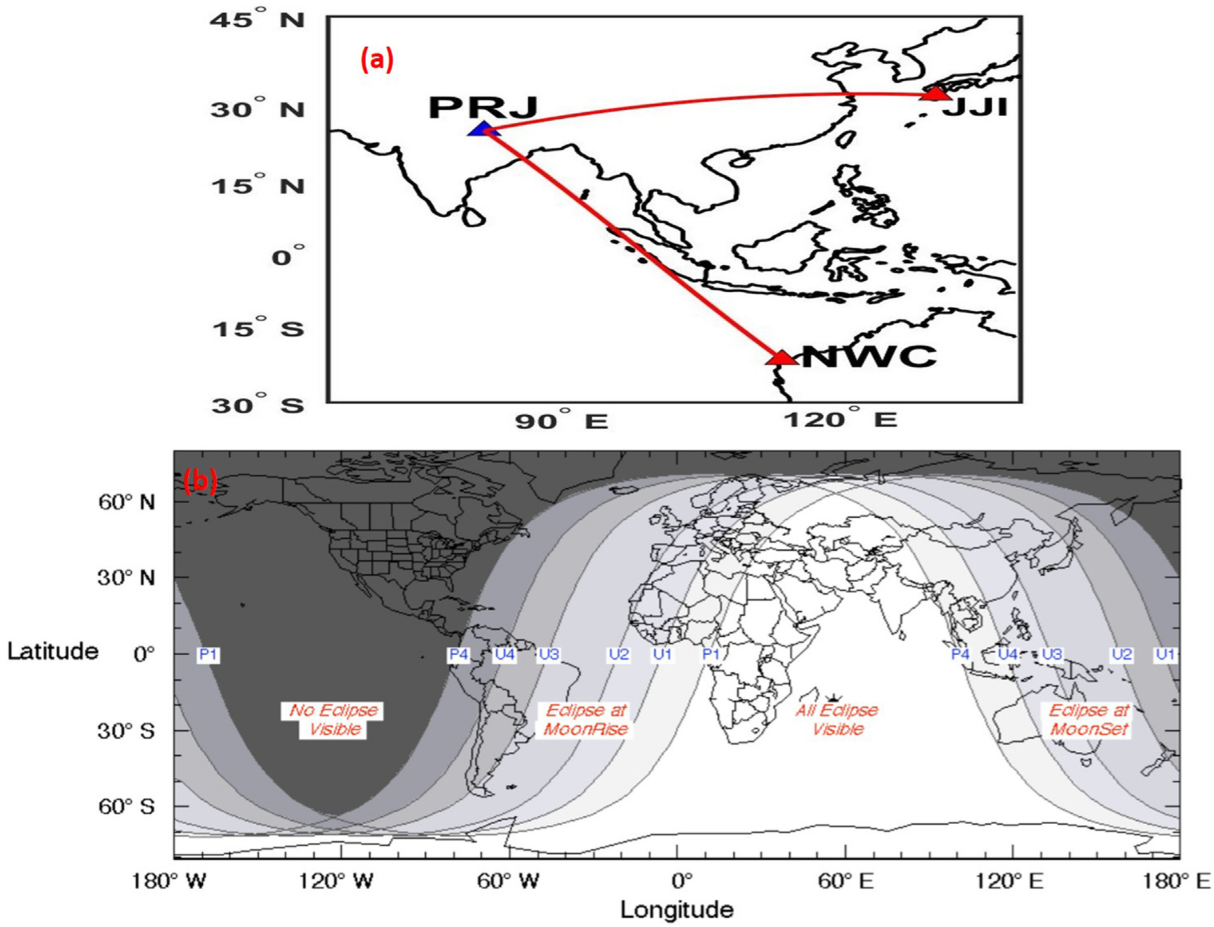

Fig. 1. **a:** Map showing location of receiving station Pryagraj (PRJ) and VLF transmitters NWC and JJI. **(b)**. Showing eclipse coverage region on the globe (obtained from NASA eclipse webpage through link (https://eclipse.gsfc.nasa.gov/LEplot/LEplot2001/LE2018Jul27T.pdf).

Table 1
Shows local the time at Prayagraj, NWC and JJI during the occurrence of eclipse.

Universal Time (UT)	Allahabad (Prayagraj), India	NWC Australia	JJI, Japan
17:14:49 (P1), 27 July	22:44:49, 27 July	01:14:49, 28 July	02:14:49, 28 July
18:24:27(U1), 27 July	23:54:27, 27 July	02:24:27, 28 July	03:24:27, 28 July
19:30:15(U2), 27 July	01:00:15, 28 July	03:30:15, 28 July	04:30:15, 28 July
21:13:12(U3), 27 July	02:43:12, 28 July	05:13:12, 28 July	06:13:12, 28 July
22:19:00(U4), 27 July	03:49:00, 28 July	06:19:00, 28 July	07:19:00, 28 July
23:28:37 (P4), 27 July	04:58:37, 28 July	07:28:37, 28 July	08:28:37, 28 July

In Table 1, P1, U1, U2, U3, U4, and P4 show the time at which the Moon passed the penumbral and umbral regions of Earth's shadow during the eclipse. The time 17:14:49 UT represented as P1 is the time at which partial lunar eclipse started and the Moon entered into the penumbral portion of the Earth's shadow. The time 18:24:27 UT represented as U1 is the time at which the Moon passed into the umbral region and the beginning of the total lunar eclipse occurred. The time 19:30:15 UT, represented by U2 is the time at which the Moon passed into the central portion of the Earth's shadow and the total lunar eclipse was at its peak. The time 21:13:12 UT which is represented by U3 is the time at which the Moon moved from the central portion of Earth's shadow. The time 22:19:00 UT, represented by U4 is the time at which the Moon moved out of the umbral portion of the Earth's shadow and the total lunar eclipse completed. The partial lunar eclipse ended when the Moon passed out of the penumbral region at 23:28:37 UT and is represented by P4.

3. Observations and modeling of the VLF signal variations during the total lunar eclipse

3.1. VLF signal amplitude variation during eclipse

To understand the impact of the total lunar eclipse on the lower ionosphere, we have utilized VLF transmitter signal (amplitude) data recorded at Prayagraj from the VLF transmitters NWC (19.8 kHz) and JJI (22.2 kHz) located in Australia and Japan respectively. We have not used phase data in this analysis as phase for both transmitters NWC and JJI on eclipse day as well as on normal days (not shown here) are erratic and hence cannot be used in analysis. The NWC and JJI transmitter signal amplitude time series plots are shown in Fig. 2 (a & b) respectively. Fig. 2 (a & b) is the average amplitude time series plots for 06 days during 24–30 July 2018, except 27 July 2018 (lunar eclipse day). As expected, clear diurnal variation of NWC and JJI signal amplitude is observed during six days for both during day and night time. The NWC diurnal mean variation (Fig. 2a) show sunrise (denoted as SR1) and two sunset terminators (denoted as SS1 and SS2) (the time at which dayside meets night side) at ∼0:20 UT, ∼10:30 UT, and ∼12:00 UT respectively. The local Indian day time (∼01–10 UT) shows smooth evolution of day time D-region ionosphere which is normally controlled by solar ionization. The nighttime (∼13–23:30 UT) signatures are highly variable due to the absence of strong daytime solar radiation. The nighttime lower ionospheric dynamics is largely controlled by highly variable nighttime sources as discussed by many previous works (e.g., Thomson et al., 2007; Ohya et al., 2011; Maurya et al., 2012). The JJI diurnal mean variation (Fig. 2b) also depict similar day/night terminator time variation but visible characteristic differs with that of NWC signal diurnal variation. The average nighttime amplitude for NWC is lower compared to the average day time NWC amplitude. While average JJI nighttime amplitude is higher than average day time JJI amplitude. Further, the NWC TRGCP show two sunset terminators (SS1 & SS2), whereas, JJI TRGCP show a single sunset terminator (SS1). This is due to different TRGCP characteristics of different time zones that affect VLF signal propagation differently (Maurya et al., 2014; Kumar and Kumar 2020).

To better understand the VLF signal amplitude variation, and for identification of anomalies due to lunar eclipse, the diurnal variation of NWC and JJI signals are shown in Fig. 3 (a & b). In Fig. 3 (a & b) the mean of 6 days (+/- 3 days of eclipse day) also considered as quiet day mean is shown with green color. Fig. 3 also includes two anomalous lines (±2σ) in black color, where σ is standard deviation values of 6 day means of VLF signal amplitude. Anything above or below black anomalous lines is considered as an anomaly. The eclipse day amplitude variation is presented by the red line. The vertical lines depict timings of Moon phases as P1, U1, U2, U3, U4 and P4. As can be seen from Fig. 3a, the NWC amplitude on eclipse day is well within the ± 2σ lines till around 14 UT, then it shows an anomalous drop in amplitude below −2σ line during ∼14–15 UT. It should be noted that this drop in amplitude appears just after SS_2 (sunset terminator time) and much before the start of the lunar eclipse, and after that it becomes normal. The first anomalous drop associated with eclipse appears at ∼17:45 UT and this drop continues for ∼27 min. The second drop appears around 18:30 UT and lasts for 20 min.

As the eclipse happened during nighttime and VLF signals are highly fluctuating, therefore in order to estimate

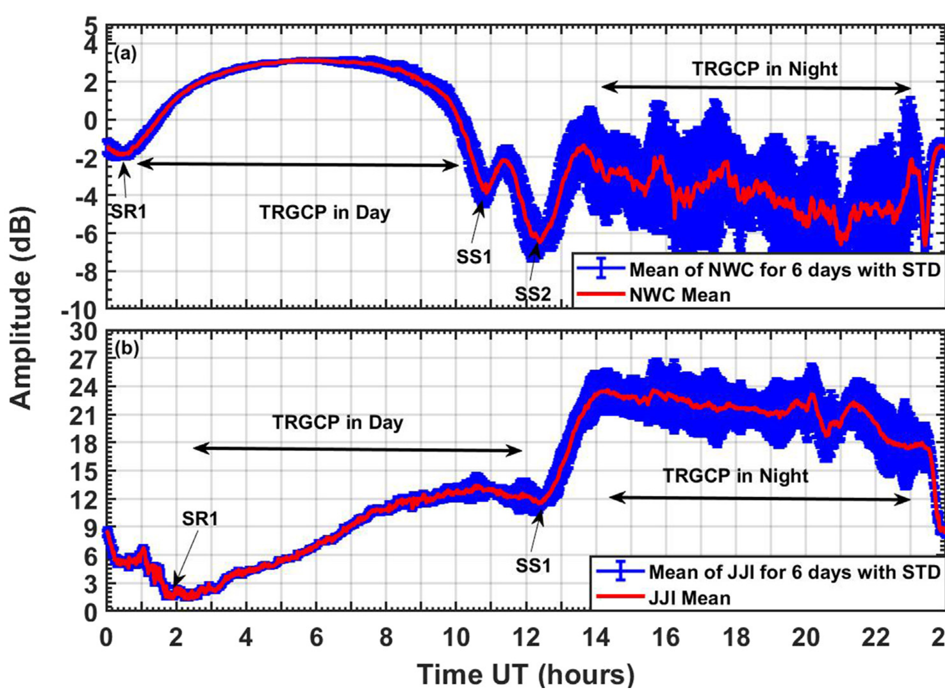

Fig. 2. **(a & b):** Showing time series variations of mean (red line) of VLF signal amplitude for NWC and JJI transmitters respectively for six days (+/- 3 days of eclipse day). The vertical lines show error bar (in blue color). The duration of TRGCP during day, night, sunrise (SR) and sunset (SS) terminator are also shown. (For interpretation of the references to color in this figure legend, the reader is referred to the web version of this article.)

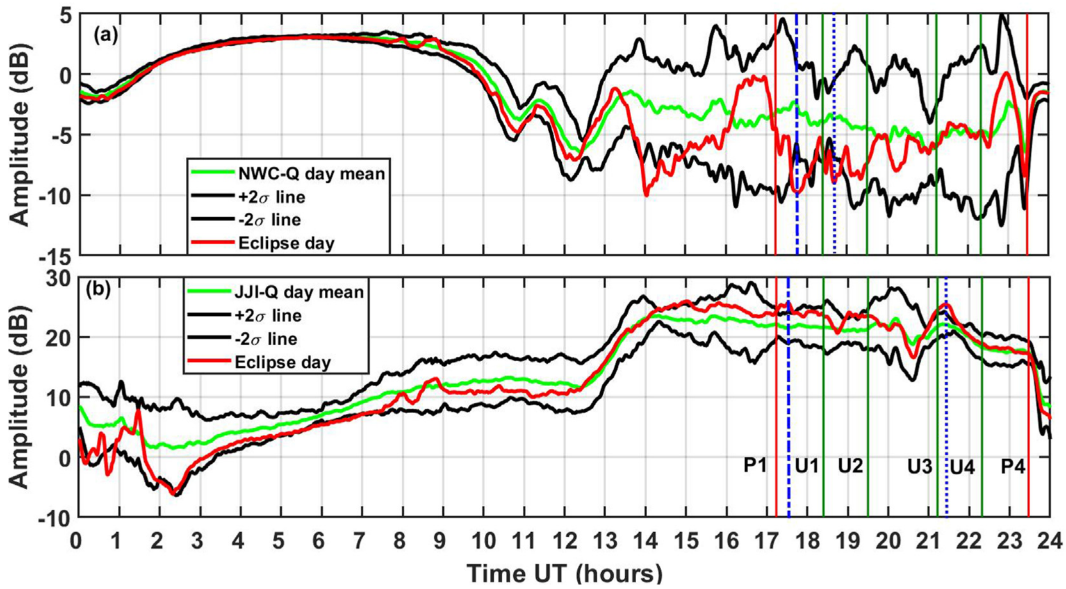

Fig. 3. **(a & b):** Show diurnal variation of mean of 6 days (green plot) also called as normal day variation, the two anomalous lines ($\pm 2\sigma$) in black color, and the eclipse day amplitude variation by red color. The vertical lines showing timing of Moon phases named as P1, U1, U2, U3, U4, and P4 along with their timing. The maximum and minimum anomalous amplitude rise/drop is shown by two vertical blue color lines, semi dashed and dashed respectively. (For interpretation of the references to color in this figure legend, the reader is referred to the web version of this article.)

eclipse related average decrease in amplitude, we have devised a method known as 'change in amplitude'. In this method, anomalous amplitude difference is calculated by subtracting maximum anomalous amplitude rise/drop to minimum anomalous amplitude rise/drop. As shown by two vertical lines (semi dashed and dashed blue lines) in Fig. 3a, the semi dashed vertical line show the time of maximum anomalous amplitude drop at ~17:46 UT with the magnitude of NWC amplitude ~9.87 dB and dashed vertical line show time of minimum anomalous amplitude drop ~18:41 UT with the magnitude of amplitude ~9.01 dB for the NWC signal, thus estimated average magnitude of change in amplitude (9.87 dB −9.01 dB) is ~0.86 dB. This method is very useful in estimating average anomalous amplitude change during nighttime when there are several anomalous decrease/increase present. For, JJI signal, as shown in Fig. 3b, the eclipse day JJI amplitude, is well within the $\pm$ 2σ lines till around ~17:10 UT, except initial drop at ~0:40 UT. The JJI signal shows the first anomalous increase at ~17:25 UT for 20 min and the second anomalous increase at ~21:20 UT for 25 min. In Fig. 3b, the semi dashed vertical line for JJI signal show time of maximum anomalous amplitude increase at ~17:31 UT with a magnitude of amplitude ~25.66 dB and dashed vertical line for JJI signal show time of minimum anomalous amplitude increase ~21:25 UT with a magnitude of amplitude ~25.4 dB. Thus, the estimated magnitude of the average change in amplitude (25.66 dB–25.04 dB) is ~0.26 dB for JJI signal. Here, it should be noted that the exact reason for anomalous drop at ~14UT in NWC signal and ~0:40 UT in JJI signal is not known. An insight into the shape of the drops shows that these are most possibly resembles Long recovery early VLF event (LORE). The LORE events are found to be associated with the transient luminous event (elves and sprites) causing D-region density perturbations as reported by Haldoupis et al. (2012). As we do not have any TLE observation and associated lightning data, thus, the events cannot be confirmed. It is to be note that the LORE events are not very well studied and understood yet, and many intriguing features are being reported time to time. In the view of the above, we plan to do a more systematic study by taking many more events in near future. Further, as the timing of these amplitude changes is outside the duration of the eclipse, thus does not affect the very main purpose of this work.

3.2. VLF signal amplitude variation during full and new Moon day

To further support our observational finding during eclipse and to better convince the readers, that the observed anomalies in VLF signals are indeed the lunar eclipse effect, we have analyzed VLF signals during a quiet full Moon (when reflected ionizing radiation is available fully) and new Moon (when there is no reflected ionizing radiation from the lunar surface) days for both JJI and NWC transmitters. For this purpose, we have explored the data availability during 2017–2018 on full Moon and new Moon day on each month. Unfortunately, we could only get 6 months data (3 month in 2018 and 3 months in 2017). The data for rest of the days was unavailable due to technical issues with the VLF receiver and non-operational of the VLF transmitters. The details for full Moon and new Moon days are obtained from https://www.calendar-12.com/moon_phases/2017. For the comparison of the effect of full Moon day to new Moon day, local nighttime (LN) is considered during 15 UT to 22 UT. The results are shown in Fig. 4.

In Fig. 4, the blue line showing full Moon day, while the red line new Moon day for JJI (left panel) and NWC (right panel) transmitter signals for 6 months (June, July, August 2017 and October, November, December 2018). Further, as the amplitude fluctuations on full and new Moon days are high, we have added in the background (light black color) 2sigma (sigma = standard deviation) variation to better understand significant amplitude fluctuations on these days. The sigma is estimated from six days mean (±3 days) around the full Moon day for each month similar to the eclipse day analysis. In general, one can see fluctuations in both transmitter signals on both days during LN. For example, the JJI signal (red line) in August 2017, showed mostly an increase during the LN above the 2sigma variation, while on new Moon day remained within the limits of 2sigma variations. The JJI signal during July 2017 on full Moon day showed an anomalous increase during the early morning time, whereas during June 2017, JJI signal on both days remained within the limits of 2sigma variations. During October and December 2018, JJI signal on both days remained within the 2sigma limit, except a few hours of LN, when the signal on new Moon day showed anomalous increase. For the month of November 2018, JJI signals on both days show an anomalous increase during LN.

The NWC signal on both days in August 2017 remained within the 2sigma limits for most of the LN time, but show an anomalous decrease (below 2sigma) around 19–21 UT. A similar variation is seen for both days of NWC signals during June 2017 and July 2017. Interestingly during October 2018, NWC signal on the new Moon day showed higher values above 2sigma limit during the initial time, then remained within the limits for subsequent hours of the LN, while the signal on the full Moon day showed an anomalous decrease during the initial hours of LN. Almost similar variation is seen on the full and new Moon days of the NWC signal during November 2018 and December 2018.

From the above discussion, it is very clear that both VLF signals on full Moon and new Moon days are not the same during LN, rather we see both increase and decrease in VLF signal on new Moon day with reference to the full Moon day. Further, a close observation indicates that for JJI signal the majority of the time, new Moon day show an anomalous increase (above 2sigma), whereas, for NWC signal, most of the time, new Moon day show an anomalous decrease (below 2sigma) with reference to the full Moon day. These results show similar features as seen in present results during eclipse day, where we see increase in JJI signal and decrease in NWC signal during eclipse time.

3.3. Modeling of VLF signals

In order to calculate the *D* region ionospheric changes (mainly the electron density) associated with signal anomalies caused by the lunar eclipse, we have adopted a method used by several researchers (e.g., Clilverd et al., 2001; Thomson et al., 2007; Maurya et al., 2014 and references therein). This method is based on estimation of *D*-region

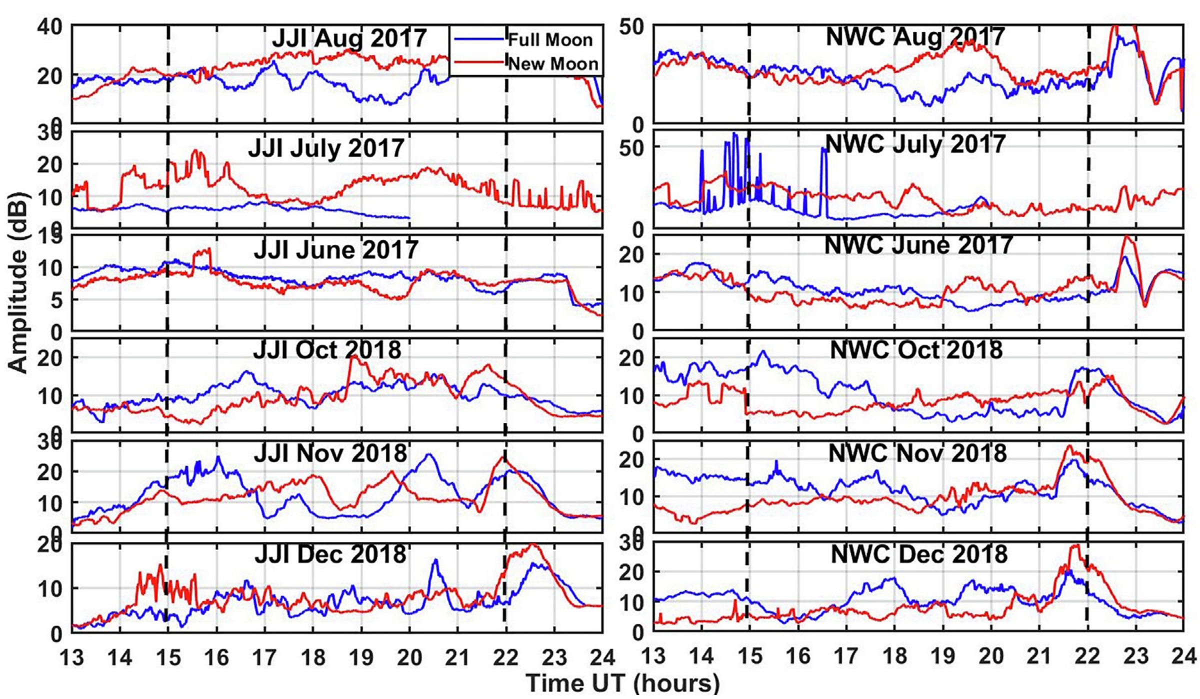

Fig. 4. Showing New Moon (red colour) and Full Moon (blue colour) variations during local nighttime for six months during 2017–2018. The left panel show JJI signal variation and right panel NWC signal variations. The background light black color show the 2sigma variation for six days (±3 days) of Full Moon day for each month. (For interpretation of the references to color in this figure legend, the reader is referred to the web version of this article.)

electron density ($N_e(z)$) profile as a function of altitude (z) by using equation

$$N_e(z) = 1.43 \times 10^7.exp\left(-0.15H'\right).\exp\left([\beta - 0.15).\left(z - H'\right)\right]el/cm^3 \quad (1)$$

where H' is D-region reference height in km and β electron density profile sharpness factor in km^{-1}. The Eq. (1) is called the Wait equation which is valid up to 100 km (Wait and Spies, 1964). The estimation of H' and β values using LWPC simulation requires precise knowledge of both amplitude and phase of the transmitter signal. As it is already stated that phase data is not useful, thus, we have used ionospheric parameter estimated by other authors for similar latitude and geomagnetic conditions. The H' and β during normal nighttime conditions were estimated by several authors (e.g., Thomson et al., 2007; Thomson and McRae, 2009; Kumar and Kumar, 2020). Thomson et al. (2007) estimated the average nighttime values of H'=85.1 km and β = 0.63 km^{-1} during low solar activity period for mid-latitude D-region ionosphere for several combinations of TRGCPs. Thomson and McRae (2009) compared the nighttime values of H' and β for equatorial and non-equatorial all-sea paths and found that the values of H'=85 km and β = 0.63 km^{-1} consistent with the previously determined values for equatorial path whereas, for *trans*-equatorial path is noticeably lower. Very recently, Kumar and Kumar, (2020) performed a detailed analysis for three combinations of TRGCPs, mainly NLK-Suva, NPM-Suva and NWC-Suva path, which covers long *trans*-equatorial high to low, mid to low and pure low latitude TRGCPs. The estimated nighttime mean values of H' and β parameters were found to be 84.2 km and 0.68 km^{-1}, respectively. After due consideration of nighttime values reported by several authors for various TRGCPs, the normal nighttime Wait parameters: H'=84.3 km and β = 0.68 km^{-1} are considered, for both NWC and JJI TRGCPs. The eclipse times H' and β are estimated by comparing changes in VLF signal amplitude. Clilverd et al. (2001) estimated that 1 dB change in the VLF signal amplitude corresponds to change in $\Delta H'$ = 1.1 km and $\Delta\beta = 0.01$ km^{-1}. They used this method and estimated values of H' and β for various combinations of TRGCPs, and results were very well reproducing observed eclipse effects. Later, this method of estimation of H' and β is successfully used by several authors (e.g., Maurya et al., 2014, 2018 and references therein) to model VLF signal amplitude perturbation during a solar eclipse. Using the same method, the H' and β values corresponding to the amplitude of NWC and JJI signals during the lunar eclipse are estimated to be H' = 85.25 km; & β = 0.689 km^{-1} for NWC signal and H' = 84.59 km & β = 0.683 km^{-1} for JJI signal. Here, it should be noted that this method of estimation of wait parameters has its own limitations. This method is very well useful in the case of the solar eclipse, which causes smooth variations in VLF signal, but as the lunar eclipse effect is not smooth rather highly variable, this method should be considered as a coarse method with the only purpose to show the difference in eclipse conditions at two signal paths may cause the different effect. This method does not provide any real change of the lunar eclipse effect. We propose here to further explore various possibilities in our future study by using a more realistic model or using LWPC code (wherever possible), and by considering the effect of various nighttime sources.

The electron density profile (N_e) is estimated using Eq. (1). By using estimated values of H' and β for normal nighttime, and during eclipse time for both NWC and JJI signals, the results are shown in Fig. 5. Fig. 5 (upper panel) show N_e profiles from 85 km to 100 km altitude, for normal nighttime (blue line), eclipse day NWC (red line) and eclipse day JJI (magenta line). It is clearly seen that NWC shows minimum N_e, while N_e for JJI is less than normal but higher than NWC. By assuming average lunar eclipse time *D*-region altitude of 85 km, there is ~40% decrease in ΔN_e for NWC path, while ~12% decrease in ΔN_e for JJI path with reference to normal nighttime N_e values. Further, we also compared N_e profile with IRI 2016 model. The IRI model estimated N_e profile is shown by thick black color for the normal day (26 July 2018) and lunar eclipse day (27 July 2018) by dashed thin green color. It is very clearly seen that IRI does not show any eclipse effect as both days (normal and eclipse day) IRI N_e plots completely overlap. Further, in order to have a better comparison, a portion of Fig. 5 (upper panel) where, IRI show comparable results with Wait profile, is zoomed and shown in Fig. 5 (lower panel). From Fig. 5 (lower panel) N_e starts increasing from zero above ~80 km altitude. From the altitude between 81 km and 88 km, the N_e values from IRI are much lower than N_e values from Wait profiles, but for the altitude range between 88 and 93 km, N_e values from both IRI and Wait show a fairly good match.

4. Discussion

The Moon affects the Earth in various ways, one of them is during lunar eclipses. During lunar eclipses, the unique geometrical alignment of the Sun, the Earth, and the Moon change the effective tidal forces. The Lunar eclipse effect on the atmosphere and ionosphere is not a widely studied phenomenon and thus very limited research papers have been published. But these limited publications give interesting clues about different atmospheric dynamical processes during lunar eclipse. As discussed earlier, Banerjee and Singh (1936) were the first to demonstrate that the *F*-region echoes become feeble during the lunar eclipse. They have suggested a possible cause as a decrease in ultraviolet radiation reflected from Moon during its blockage by the Earth. Stetson (1944), reported the effect of the total lunar eclipse of October 28, 1939, on the ionization of the E-layer (~100 km altitude) by analyzing field intensity of WBBM Chicago at 770 kHz frequency recorded at MIT at Boston. The observed rapid rise in field

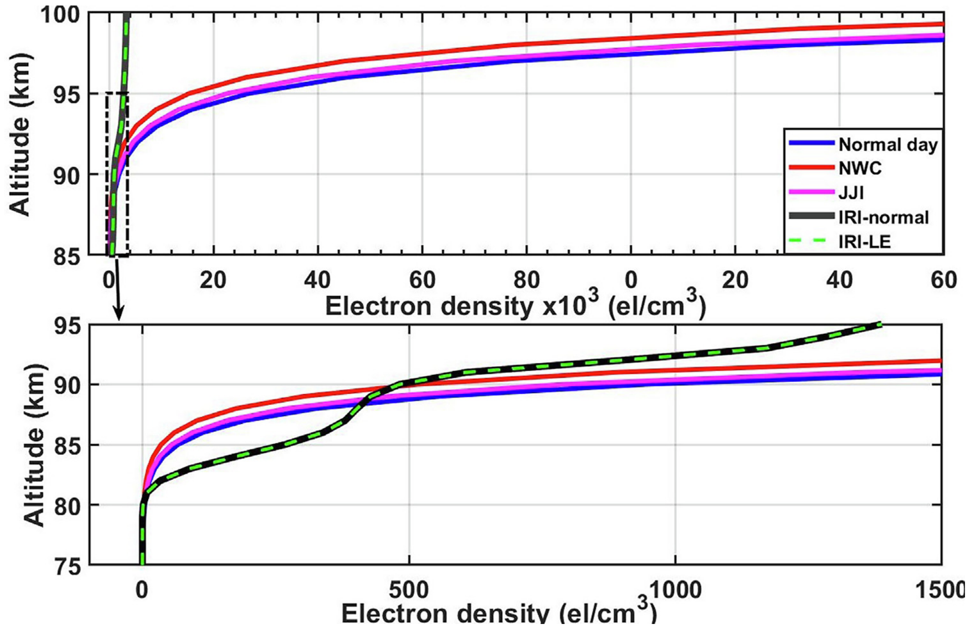

Fig. 5. **(upper panel)** Show N_e profile from 85 km to 100 km altitude estimated using wait parameters calculated through modeling of VLF signals. The normal nighttime profile is shown by blue plots while red and magenta plots are anomalous variation of NWC and JJI signals respectively. The IRI model estimated N_e profile is shown by thick black color for normal day (26 July 2018) and lunar eclipse day (27 July 2018) by dashed thin green color. The zoomed portion is shown as **(lower panel)** with altitude from 75 to 95 km. (For interpretation of the references to color in this figure legend, the reader is referred to the web version of this article.)

intensity of WBBM Chicago when Moon enters the umbral shadow which followed by a drop in intensity as the eclipse progressed further. This sudden rise in field intensity was explained on the basis of reduction in attenuation due to increasing recombination due to cutting off of ionizing radiation from Moon.

In the present work, the focus is on the night time lower ionosphere in the altitude range of 80–90 km, which is being probed using very low frequency waves from two transmitter signals JJI (22.2 kHz) from Japan and NWC (19.8 kHz) from Australia. The NWC-Prayagraj TRGCP‘s most part was is in the totality region and showed anomalous decrease in signal amplitude during eclipse. Whereas JJI-Prayagraj TRGCP's most part was in the partial eclipse region and showed a small increase in signal amplitude. Past observations of day time solar eclipse (e.g. Clilverd et al., 2001; Maurya et al., 2014; Venkatesham et al., 2019) showed similar changes i.e. both decrease and increase in VLF signal amplitude during the same eclipse. Clilverd et al. (2001) during 11 August 1999, total solar eclipse studied various combinations of TRGCPs (∼17 paths) and reported both positive and negative amplitude changes associated with the solar eclipse. Maurya et al. (2014) studied effect of 22 July 2009 total solar eclipse effect on the lower ionosphere using JJI signal recorded at five stations covering path of totality, and reported increase in JJI signal amplitude due to eclipse. Whereas, Venkatesham et al. (2019) used NWC signal recorded at these five stations and reported decrease in amplitude associated with 22 July 2009 total solar eclipse. It is suggested that the increase/decrease in signal amplitude is the result of modal interference at the receiving station, which depends on various factors such as TRGCP path length, orientation, path types etc. It is interesting to note that, increase in JJI amplitude and decrease in NWC amplitude as reported by Maurya et al. (2014) and Venkatesham et al. (2019) for 22 July 2009 total solar eclipse is also seen in the present case of the total Lunar eclipse of 27 July 2018. This might also be related with the diurnal variation of JJI and NWC signal at receiving station Prayagraj. As shown in Fig. 2 and discussed in Section 3.1 for the NWC signal, the average nighttime amplitude is lower in comparison to the average day time amplitude, while for JJI signal, the average nighttime amplitude is higher than the average day time amplitude. Thus, during lunar eclipse, when ionization density decrease, as compared to non-eclipse days (normal days), JJI signal show increase while NWC signal show decrease.

Further, the comparison of full Moon (when reflected ionizing radiation is available fully) day and new Moon (when there is no reflected ionizing radiation from the lunar surface) day as shown in Fig. 4 and discussed in Section 3.2, further supports the present observations of lunar eclipse effect in VLF signals. We see both increase and decrease in VLF signal on new Moon day with reference to the full Moon day, but for JJI signal majority of time, new Moon day show increase, whereas, for NWC signal, most of the time, new Moon day show decrease with reference to the full Moon day. These are the similar feature as seen during lunar eclipse day, where JJI signal show increase and NWC signal show decrease during eclipse time. As mentioned in the introduction, similar observations were also reported by Stetson 1944, who reported change in WBBM Chicago signal at 770 kHz frequency associated with changing phases of the Moon.

Further, VLF signal modeling of normal nighttime and eclipse time showed an increase in the Wait's lower ionospheric parameters *H'* and β for both NWC and JJI as compared to normal nighttime values. Previous observations during the total solar eclipse, also show a similar increase in the Wait's parameters (Clilverd et al., 2001; Maurya et al., 2014). The increase in Wait parameters signifies a decrease in lower *D*-region ionosphere electron density. We also see a similar decrease in *D*-region electron density but for the total lunar eclipse which are essentially associated with the nighttime.

The estimated N_e profile during total lunar eclipse using modeled Wait's parameters showed a maximum decrease in NWC path, while less decrease for JJI path. This is possibly due to the facts that NWC TRGCP is exposed to a higher duration of the total lunar eclipse as compared to JJI TRGCP. The N_e profiles from the IRI model do not show any eclipse effect and also N_e values are very small compare to N_e values obtained using the Wait's equation. This indicates further improvements are needed in the IRI model to account for the nighttime *D*-region N_e values. Overall, observations clearly show a change in signal amplitude indicating a decrease in the nighttime electron density. Though the magnitude of decrease in N_e is very small but could be useful to understand changes in the dynamical processes of the lower ionosphere during the lunar eclipses.

The nighttime lower ionosphere is very weakly ionized plasma due to the absence of main ionizing radiation from the Sun. As discussed by Ohya et al. (2011) and Maurya et al. (2012), in the absence of the main source of ionization, various minor source such as geocorona emission, reflected X-rays, galactic cosmic rays, particle precipitation, reflected lunar light produces observed ionization during the nighttime. Each source produces ionization to different extent, which is not yet exactly quantified, thus, we see a highly variable nighttime VLF signal. Therefore, unlike the solar eclipse, a smooth drop in VLF signal amplitude following the lunar eclipse variations could not be observed. Interestingly, we have observed higher drop in NWC signal during penumbra compare to during the total eclipse. The most probable reason could be related to the dominant source of ionization during that time. It is possible that other sources are dominating during eclipse totality time, and we do observe smaller change. Further, as suggested by Thomson et al. (2007) and Ohya et al. (2011), the Lyman-α from geocorona remains the major source of ionization for nighttime lower ionosphere ionizing NO and O_2. As reported in many previous works (e.g., Carver et al., 1974; Lucke et al., 1976; Taguchi et al., 2000) the spectrum of Lunar albedo also contains Lyman-α radiation that might also be contributing to the nighttime D-region ionization. Lucke et al. (1976), measured the geometrical albedo of the Moon in the far-ultraviolet (FUV) between 121.6 nm and 168 nm. They compared the Moon brightness, from far-ultraviolet spectrometer onboard the Apollo17 mission to the solar brightness from a sounding rocket. The observed albedo at Lyman-α was found to be ~0.063 (~6.3%). Taguchi et al. (2000), also estimated geometric albedo of the Moon ~5.2% at Lyman α wavelength using an imaging observation by the ultraviolet imaging spectrometer (UVS) during the lunar encounter of the NOZOMI spacecraft. Thus, the observations suggest that a significant amount of Lyman-α (albedo varies from 3 to 6% depending on the lunar surface) is present in the reflected lunar light.

Further, it is well known that the solar X-rays in the wavelength range of 0.2–0.8 nm (1.5–6 KeV energy) ionizes neutral constituents along with the major constituents O_2 and N_2 of the D-region ionosphere (Mitra, 1974). Several past measurements show significant X-rays emission from the Moon surface (e.g. Schmitt et al. 1991 and reference therein; Kamata et al., 1999; Bhardwaj et al., 2007). Schmitt et al. (1991), using observations from the PSPC instrument onboard ROSAT satellite found the X-ray emission above the Cosmic X-ray Background (CXB) by the Moon, in the 0.1–2 keV energy band. Even the dark side of the Moon shows an excess emission component ~2 orders of magnitude weaker than the bright side component. They suggested that X-ray emissions results from energetic solar wind electron striking Moon's surface. Kamata et al. (1999) analyzed the results obtained from ASCA (Japanese X-ray astronomy satellite) observation of the lunar surface, which shows significant observations of fluorescence X-rays from the lunar surface. Hence reflected X-rays from the Moon surface may also contribute in the nighttime ionization of the lower ionosphere.

As discussed earlier, such a possibility of the lunar effect on the ionosphere was hypothesized by Stetson (1944), who suggested that the ionizing radiation from the Moon, mainly emission of secondary X-ray radiation and reflected ultra-violet radiation may cause the change in field intensity of WBBM Chicago at 770 kHz frequency changes the ionization of the E-layer (~100 km altitude). Such ionization depends upon the amount of Moon's surface directed towards the radio signal path. Therefore, results from the above discussions of previous observations suggest that reflected lunar radiation comprises significant portion of Lyman-α and X-rays, major ionizing radiations of the D-region. Hence, during the lunar eclipse when the earth is in between the sun and the Moon thereby blocking the solar radiation reaching Moon, and thus reflected lunar Lyman-α and X-rays radiation, leading to further decrease in the nighttime lower ionospheric electron density, below the ambient level. It should be noted that quantitative estimation of the lunar reflected radiation is not yet available, therefore, at present it is difficult to quantify and attribute the observed changes in the VLF signal amplitude is due to the changes in the reflected radiation from the Moon during the lunar eclipse. More study and modeling work is required to clearly understand lunar contribution in the nighttime lower ionosphere. Further, such information would be very useful in the future radio wave propagation models that may be utilized to produce effective radio communication and navigation.

5. Summary

The results presented here are first of its kind observations and modeling work is done to understand the effect of the total lunar eclipse on the lower ionosphere using VLF waves from low latitude region. The VLF signals from two navigational transmitters NWC from Australia and JJI from Japan was recorded at VLF receiving station Prayagraj (formally Allahabad) in India. The total lunar eclipse of 27 July 2018 was the longest lunar eclipse of the 21st century, thus provides an obvious interest to study its effect on the lower ionosphere. Our analysis of VLF signal amplitude showed an anomalous decrease in NWC amplitude, and an increase in JJI amplitude. It is observed that magnitude of increase for JJI signal was less compared to magnitude of decrease in NWC amplitude. The TRGCP of JJI was in partial eclipse region. Whereas TRGCP of NWC was mostly in the total lunar eclipse region. These observations were also supported by variations of VLF signals during new Moon days with reference to full Moon days. The JJI signal for most of the time show increase whereas NWC signal show decrease on new Moon day compare to full Moon day similar to the observed lunar eclipse effect in both signals. A coarse method of modeling is being used and estimate Wait parameters H' and β showed an increase for both NWC and JJI signals when compared to normal control nighttime values. The N_e values for the NWC path showed a relatively higher decrease compared to JJI path. Though the decrease in N_e during the lunar eclipse is small, but could be useful to understand nighttime D-region dynamical processes during the total lunar eclipse. Our analysis further suggests that the likely possibility for such decrease in N_e could be due to reflected lunar Lyman-α and X-rays radiation which is blocked during the lunar eclipse, thereby decreasing the nighttime lower ionospheric density with reference to ambient nighttime value. The work also signifies important role of VLF signals in detecting even smallest change (due to lunar eclipse) in lower ionosphere monitoring.

Declaration of Competing Interest

The authors declare that they have no known competing financial interests or personal relationships that could have appeared to influence the work reported in this paper.

Acknowledgments

The authors would like to extend gratitude to Director, Indian Institute of Geomagnetism for providing necessary support and encouragement to carry out research. AKM thanks Science and Education Research Board for financial support under Ramanujan Fellowship (File No SB/S2/RJN-052/2016) and Faculty Recharge Program (FRP) of University Grant Commission (UGC) (ID FRP62343), New Delhi. KV thanks Science and Education Research Board for financial support under National Post Doctoral Fellowship (File No PDF/2019/002507).

References

Anderson, R.C., Keefer, D.R., Myers, O.E., 1972. Atmospheric pressure and temperature changes during the 7 March 1970 solar eclipse. J. Atmos. Sci. 29, 583–587.

Antonia, R.A., Chambers, A.J., Phong-Anant, D., Rajagopalan, S., Sreenivasan, K.R., 1979. Response of atmospheric surface layer turbulence to a partial solar eclipse. J. Geophys. Res. 4, 1689–1692. https://doi.org/10.1029/JC084iC04p01689.

Banerjee, S.S., Singh, B.N., 1936. Effect of Lunar Eclipse on the Ionosphere. Nature.

Bhardwaj, A., Elsner, R.F., Gladstone, G.R., Cravens, T.E., Lisse, C.M., Dennerl, K., Branduardi-Raymont, G., Wargelin, B.J., Waite Jr., J.H., Robertson, I., Østgaard, N., Beiersdorfer, P., Snowden, S.L., Kharchenko, V., 2007. X-rays from Solar System Objects. Planet. Space Sci. 55, 1135–1189.

Carver, J.H., Horton, H.B., O'Brien, R.S., O'Connor, G.G., 1974. The ultraviolet reflectivity of Moon. Moon 9, 295–303.

Chimonas, G., 1970. Internal gravity-wave motion induced in the Earth's atmosphere by a solar eclipse. J. Geophys. Res. 75 (28), 5545–5551. https://doi.org/10.1029/GM018p0708.

Chimonas, G.C., Hines, O., 1970. Atmospheric gravity waves induced by a solar eclipse. J. Geophys. Res. 75, 857–875. https://doi.org/10.1029/JA075i004p00875.

Clilverd, M.A., Rodger, C.J., Thomson, N.R., Lichtenberger, J., Steinbach, P., Cannon, P., Angling, M.J., 2001. Total solar eclipse effects on VLF signals: Observation and modeling. Radio Sci. 36 (4), 773–788. https://doi.org/10.1029/2000RS002395.

Cohen, M.B., Inan, U.S., Paschal, E.W., 2010. Sensitive broadband ELF/VLF radio reception with the AWESOME instrument. IEEE Trans. Geosci. Remote Sens. 47. https://doi.org/10.1109/TGRS.2009.2028334.

Pallé, E., Osorio, M.R.Z., Barrena, R., Montañés-Rodríguez, P., Martín, E.L., 2009. Earth's transmission spectrum from lunar eclipse observations. Nature 459. https://doi.org/10.1038/nature08050.

Haldoupis, C., Cohen, M., Cotts, B., Arnone, E., Inan, U., 2012. Long-lasting D-region ionospheric modifications, caused by intense lightning in association with elve and sprite pairs. Geophys. Res. Lett. 39, L16801. https://doi.org/10.1029/2012GL052765.s.

Kamata, Y., Takeshima, T., Okada, T., Terada, K., 1999. Detection of X-ray fluorescence like features from the Lunar surface. Adv. Space Res. 23 (11), 1829–1832.

Kawauchi, K., Narita, N., Sato, B., Hirano, T., Kawashima, Y., Nakamoto, T., Yamashita, T., Tamura, M., 2018. Lowest Earth's atmosphere layers probedduring a lunar eclipse, 70, 84. Earth Plane. Astrophys. https://doi.org/10.1093/pasj/psy079.

Kumar, A., Kumar, S., 2020. Ionospheric D region parameters obtained using VLF measurements in the South Pacific region e2019JA027536. J. Geophys. Res. Space Phys. 125. https://doi.org/10.1029/2019JA027536.

Lucke, R.L., Henry, R.C., Fastie, W.G., 1976. Far-ultraviolet albedo of the Moon. Astron. J. 81 (12), 1162–1169.

Maurya, A.K., Veenadhari, B., Singh, R., Kumar, S., Cohen, M.B., Selvakumaran, R., Gokani, S., Pant, P., Singh, A.K., Inan, U.S., 2012. Nighttime D region electron density measurements from ELF-VLF tweek radio atmospherics recorded at low latitudes. J. Geophys. Res. 117, A11308. https://doi.org/10.1029/2012JA017876.

Maurya, A.K., Phanikumar, D.V., Singh, R., Kumar, S., Veenadhari, B., Kwak, Y.S., Kumar, A., Singh, A.K., Niranjan Kumar, K., 2014. Low-mid latitude D region ionospheric perturbations associated with

22 July 2009 total solar eclipse: Wave-like signatures inferred from VLF observations. J. Geophys. Res. Space Physics 119. https://doi.org/10.1002/2013JA019521.

Maurya, A.K., Venkatesham, K., Kumar, S., Singh, R., Tiwari, P., Singh, A.K., 2018. Effects of St. Patrick's Day geomagnetic storm of March 2015 and of June 2015 on low-equatorial D region ionosphere. J. Geophys. Res. Space. Physics 123. https://doi.org/10.1029/2018JA025536.

Mitra, A.P., 1974. Ionospheric Effects of Solar Flares. D. Reidel Publishing Company, Dordrecht-Holland.

Ohya, H., Shiokawa, K., Miyoshi, Y., 2011. Long-term variations in tweek reflection height in the D and lower Eregions of the ionosphere. J. Geophys. Res. 116, A10322. https://doi.org/10.1029/2011JA016800.

Phanikumar, D.V., Kwak, Y.S., Patra, A.K., Maurya, A.K., Singh, R., Parke, S.M., 2014. Response of the mid-latitude D-region ionosphere to the Total Solar Eclipse of 22 July 2009 studied using VLF signals in South Korean peninsula. Adv. Space Res. 54, 961–968.

Schmitt, J.H.M.M., Snowden, S.L., Aschenbach, B.A., Hasinger, G., Pfeffemtann, E., Pradehl, P., Trumper, J., 1991. A soft X-ray image of the Moon. Nature 349, 583–587.

Singh, R., Veenadhari, B., Maurya, A.K., Cohen, M.B., Kumar, S., Selvakumaran, R., Pant, P., Singh, A.K., Inan, U.S., 2011. D-region ionosphere response to the Total Solar Eclipse of 22 July 2009 deduced from ELF-VLF tweek observations in the Indian sector. J. Geophys. Res. 116, A10301. https://doi.org/10.1029/2011JA016641.

Singh, R., Veenadhari, B., Cohen, M.B., Pant, P., Singh, A.K., Maurya, A.K., Vohat, P., Inan, U.S., 2010. Initial results from AWESOME VLF receivers: Setup in low latitude Indian region under IHY2007/UNBSSI program. Curr. Sci. 98 (3), 398–405.

Srivastava, G.P., Pakkir, M., Balwalli, R.R., 1982. Ozone concentration measurements near the ground at Raichur during the solar eclipse of 1980. Proc. Indian Natl. Sci. Acad A48 (3), 138–142.

Stetson, H.T., Johnson, J., 1934. On the possibilities of a tidal effect in the Kennelly-Heavtside Layer as evidenced by an apparent correlation of the intensity of radio reception with positions of the Moon. Terr. Mag. 39, 145–158.

Stetson, H.T., 1931. On the correlation of radio reception with the Moon's position in the observer's sky. Terr. Mag. 36, 1–5.

Stetson, H.T., 1944. On the Observational Evidence for Changes in Ionization of the Upper Atmosphere Attributable to the Moon. Terr. Mag. & Atom. Elec. 49, 9–24.

Taguchi, M., Funabashi, G., Watanabe, S., Takahashi, Y., Fukunishi, H., 2000. Lunar albedo at hydrogen Lyman α by the NOZOMI/UVS. Earth Planets Space letters 52, 645–647.

Thomson, N.R., McRae, W.M., 2009. Nighttime ionospheric D region: Equatorial and nonequatorial. J. Geophys. Res. 114, A08305. https://doi.org/10.1029/2008JA014001.

Thomson, N.R., Clilverd, M.A., McRae, W.M., 2007. Nighttime ionospheric D region parameters from VLF phase and amplitude. J. Geophys. Res. 112, A07304. https://doi.org/10.1029/2007JA012271.

Venkatesham, K., Singh, R., Maurya, A.K., Dube, A., Kumar, S., Phanikumar, D.V., 2019. The 22 July 2009 total solar eclipse: Modeling D region ionosphere using narrowband VLF observations. J. Geophys. Res. Space Phys. 124. https://doi.org/10.1029/2018JA026130.

Wait, J.R., Spies, K.P., 1964. Characteristics of the earth-ionosphere waveguide for VLF radio waves. Tech. Note 300, Nat. Burr. Of Stand., Boulder, Colo.